ISSN 0020-1685, Inorganic Materials, 2015, Vol. 51, No. 8, pp. 840–847. © Pleiades Publishing, Ltd., 2015.
Original Russian Text © S.N. Ivicheva, Yu.F. Kargin, V.S. Gorelik, 2015, published in Neorganicheskie Materialy, 2015, Vol. 51, No. 8, pp. 914–922.

Opal-Matrix Nanocomposites Containing Metallic Nanoparticles

S. N. Ivicheva[a], Yu. F. Kargin[a], and V. S. Gorelik[b]

[a] *Baikov Institute of Metallurgy and Materials Science, Russian Academy of Sciences, Leninskii pr. 49, Moscow, 119991 Russia*
e-mail: yu.kargin@rambler.ru

[b] *Lebedev Physical Institute, Russian Academy of Sciences, Leninskii pr. 53, Moscow, 119991 Russia*
e-mail: gorelik@sci.lebedev.ru

Received December 25, 2014

Abstract—A method has been proposed for the fabrication of three-dimensional photonic crystals based on ordered opal matrices (OMs), with pores containing iron group metal (M = Ni, Co, Fe) nanoparticles. The core of the method is the reduction of salts and oxides of these metals with supercritical isopropanol. The phase composition of OM/M composites depends on the composition of the starting salts (nitrates or chlorides): the use of ferric chloride leads to the formation of nanoparticles of solid solutions based on nickel metal, α-cobalt, or β-cobalt (Ni–Fe and Co–Fe systems) in opal pores; with the corresponding nitrates, we obtain OM/NiCo (cubic solid solution), OM/Fe, OM/Ni_3Fe, OM/NiFe, OM/CoFe, and OM/NiCoFe nanocomposites. We have measured broadband reflection spectra of the (111) surface of the photonic crystals using a fiber-optic technique for taking reflection spectra. The intensity peak in the reflection (band gap) spectrum of the OM/M (M = Fe, Co, Ni) nanocomposites is shown to be shifted to longer wavelengths.

DOI: 10.1134/S0020168515070080

INTRODUCTION

Recent years have seen rapid growth of nanotechnologies related to the fabrication and practical application of ordered three-dimensional nanostructures—three-dimensional photonic crystals [1–5]. Typical examples of such nanostructures are opal matrices (synthetic opal) built up of close-packed amorphous quarts (silica) spheres 200 to 600 nm in size. The crystal structure of such opal photonic crystals has a face-centered cubic lattice. Between the close-packed nanospheres in opal, there are tetrahedral and octahedral pores (voids). The volume fraction of the pores in opal is about 0.26. The relative radii (relative to the radius of the SiO_2 spheres) of spherical nanoparticles that can be embedded in the opal pores are 0.23 and 0.41 for the tetrahedral and octahedral pores, respectively.

The opal pores can be filled with a variety of substances. The simplest approach is to impregnate synthetic opal with liquids that wet quartz: water, alcohols, acetone, and others. Filling the opal pores with saturated solutions of salts or aromatic compounds in such liquids, followed by evaporation of the solvent in the opal pores, leads to the precipitation of the respective compounds: salts, aromatic substances, etc. [6]. Attempts to fill opal pores with metals or oxides pose more serious problems [7]. Iron-group metal nanoparticles can be prepared by a variety of methods: thermolysis of metalorganic compounds [8–10], electrochemical [11] and chemical deposition [12, 13], and in colloidal chemical systems with reverse micelles as micro- and nanoreactors [14, 15] that can be used for embedding in mesoporous silica. In particular, nickel nanoparticles can be embedded in mesoporous silica using inorganic and organic salts (nickel nitrates, sulfates, chlorides, bromides, amine chlorides, and amine nitrates, as well as nickel acetate, acetylacetonate, and citrate) [16]. Ni nanowires in channels of anodized aluminum oxide can be produced by metal electrocrystallization at a constant potential [17]. Cobalt-containing nanocomposites can be prepared using cobalt carbonyl and various salts: $Co_2(CO)_8$, $Co(NO_3)_2$, and $Co(Ac)_2$. Cobalt is introduced in the form of cobalt-containing compounds or preprepared metal nanoparticles during the synthesis of a mesoporous matrix, by impregnating it with salt solutions, followed by reduction in the liquid phase [18]. Magnetic nanocomposites containing filamentary iron and iron oxide nanoparticles in a mesoporous silica matrix are commonly prepared by embedding iron pentacarbonyl, acetylacetonate, or citrate into the hydrophobic or hydrophilic part of SiO_2/template composite micelles, followed by crystallization in flowing hydrogen at temperatures from 250 to 700°C [19]. Fe–Co and Fe–Ni solid solution nanoparticles can be prepared by reducing solutions of their salts with hydrazine hydrate in an alkaline medium [12, 20, 21]. $FeNi_3$ nanoparticles were prepared by a hydrothermal process [22]. There are also reports on the preparation of monodisperse spherical iron particles [23], Co dendrites [20], magnetite tetrapods [24], multi-

layer FeCo structures [25], and core/shell bimetallic particles [26].

Liquid metals can be infiltrated into synthetic opal pores at high pressures and temperatures by magnetron sputtering [27], ultrasonic processing [28], laser ablation [29], chemical deposition [8, 30], and electrolysis [31]. With these techniques, however, substances are only incorporated into a thin surface layer of opal crystals.

Refractory metals and oxides can be incorporated into opal pores by reducing appropriate salts in opal with alcohols in a supercritical state [32–35]. As shown in experimental studies [32–35], reactions of supercritical alcohols with salts and oxides have a reducing character, ensuring the formation of refractory metal or oxide nanoparticles in opal pores.

It is known that the key property of photonic crystals is the presence of band gaps, which are responsible for the anomalous reflection of electromagnetic radiation from the surface of a three-dimensional photonic crystal in the spectral region corresponding to the position of a band gap. At typical sizes of spheres in synthetic opal (200–400 nm), the band gaps of opal crystals fall into the visible range.

Gorelik [5, 36] and Voinov et al. [37] developed an effective technique for obtaining the spectrum of the band gaps of photonic crystals with high spatial resolution using fiber optics. It involves a local analysis of broadband reflection spectra of the (111) surface of a three-dimensional photonic crystal at normal incidence of light on this surface and in backscattering geometry. Such experiments, with the use of a halogen or deuterium lamp as a broadband light source, allow one to determine characteristics of the first and second band gaps in the [111] crystallographic direction of the photonic crystal.

The objectives of this study were to produce new types of opal-matrix (OM) nanocomposites containing iron-group refractory metal (M = Ni, Co, Fe) nanoparticles prepared by reducing appropriate salts or oxides with supercritical alcohols [32–35] and to obtain broadband reflection spectra of the (111) surface of the photonic crystals using a fiber-optic technique developed previously [5, 36, 37] for measuring reflection spectra, in order to find characteristics of the band gaps of the nanocomposites.

EXPERIMENTAL

Fabrication of opal-matrix composites containing iron group metal nanoparticles. The starting chemicals used to prepare the solutions to be infiltrated into opal were the crystalline hydrates $Ni(NO_3)_2 \cdot 6H_2O$ (analytical grade), $Co(NO_3)_2 \cdot 6H_2O$ (analytical grade), $Fe(NO_3)_3 \cdot 9H_2O$ (analytical grade), and $FeCl_3 \cdot 6H_2O$ (analytical grade). Opal/metal nanocomposites had the form of opal matrices consisting of SiO_2 spheres, with opal pores containing 3*d* transition metal nanoparticles (Fe, Co, Ni, and their binary and ternary combinations: alloys and solid solutions) synthesized as described previously [32–35]. Opal crystals containing nanoparticles of various metals were prepared as described elsewhere [38]. Opal consisting of monodisperse silica spheres 270–280 nm in size was infiltrated with concentrated (50%) water–alcohol solutions of Co, Ni, and Fe(III) salts (nitrates and chlorides) and with mixed solutions of iron group metal salts in various proportions for the Co:Ni, Co:Fe, and Ni:Fe binary systems and in the Co:Ni:Fe (1 : 1 : 1) ternary system. The samples thus prepared were dried at room temperature (t_R) and then heat-treated at 450°C to a preset schedule. Next, the samples were exposed to supercritical isopropanol at temperatures from 250 to 300°C and a pressure on the order of 10 MPa in 200-cm^3 steel autoclaves.

The phase composition of the unfilled opal and nanocomposites was determined after each processing step by X-ray diffraction on a Shimadzu XRD 6000 diffractometer (λ_{Cu}= 1.54184 Å). The crystallite size (D_{cr}) of crystalline phases in the X-ray amorphous opal was evaluated from X-ray diffraction data using the Scherrer formula. Unit-cell parameters were determined by least squares extrapolation. The phases present were identified using JCPDS–ICDD PDF data (release 2003) [39].

The morphology and size of the nanoparticles in the opal matrix were assessed by scanning electron microscopy (SEM) on a Carl Zeiss Model NVision 40 and a JEOL JSM-7001F electron microscope equipped with Oxford Instruments X-ray microanalysis systems.

Fiber-optic technique for local analysis of the spectrum of band gaps in the nanocomposites. In this study, we used as-prepared opal consisting of monodisperse spheres about 270 nm in diameter. The opal had the form of 2- to 4-mm-thick plane-parallel plates ≃1 cm^2 in area, with (111)-oriented faces. Figure 1 shows a block diagram of the experimental setup used. Spectra were analyzed in backscattering (180°) geometry. Broadband radiation from a radiation source (*1*) (halogen lamp) was delivered by an optical fiber (*2*) secured in a probe (*4*) to the (111) surface of a sample under study (*5*). A diaphragm (*6*) ensured localization of the radiation under study on a small surface area of the nanocomposites being investigated. Another optical fiber (*3*) was used to deliver the reflected light to an FSD8 minispectrometer, which was connected to a computer (*8*). From the minispectrometer, reflection spectra in digital form were fed to the computer through a USB cable. The optical and spectral characteristics of the spectrometer ensured high sensitivity in spectral measurements. The spectra were obtained at exposure times from 100 μs to 32 s.

The fiber-optic setup built for measurements of local reflection spectra enabled parameters of the band gaps of opal crystals to be determined with a 0.2-mm

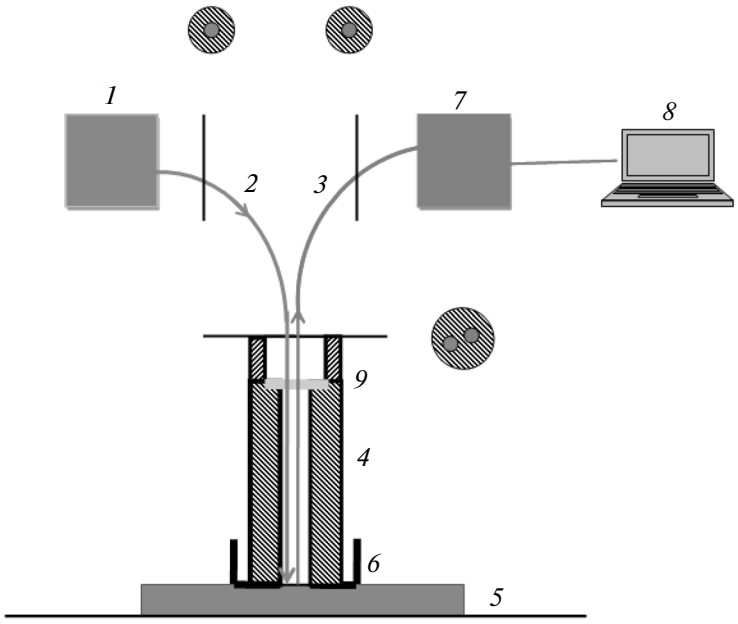

Fig. 1. Block diagram of the experimental setup used to measure local reflection spectra of the (111) surface of opal: (*1*) light source, (*2*, *3*) optical fibers, (*4*) Y-shaped probe, (*5*) photonic crystal under study, (*6*) diaphragm, (*7*) minispectrometer, (*8*) computer, (*9*) transparent transition layer.

spatial resolution on the surface of the nanocomposite photonic crystals and a spectral resolution of ≃1 nm.

RESULTS AND DISCUSSION

Treatment of opal with supercritical isopropanol after a single cycle of filling the opal pores with 50% solutions of Co, Ni, and Fe salts (or solutions of two or three components in certain ratios) and subsequent thermal decomposition of the salts allowed us to obtain nanocomposites with the following phase compositions: OM/Co (α-Co (89-4308), β-Co (89-4307)), OM/Ni (Ni (87-0712)), OM/Fe(Cl) (Fe_3O_4 magnetite (19-0629), γ-Fe_2O_3 (39-1346)?), OM/Fe(N) (Fe (6-0696), Fe (1-1252), Fe_3O_4 magnetite (19-0629)), OM/Ni:Co (1 : 1) (NiCo solid solution); OM/Ni:Co (1 : 2) (NiCo solid solution, α-Co (89-4308) hex), OM/Ni:Fe(Cl) (1 : 1) (Fe_3O_4 (19-0629), Ni (87-0712)), OM/Ni:Fe(N) (1 : 1) ($FeNi_3$ (65-3244), Fe_3O_4 (19-0629)), OM/Co:Fe(N) (1 : 1) (β-Co (15-0816), Fe_3O_4 (19-0629)), OM/Co:Fe(N) (1 : 2) (β-Co (15-0816), Fe (6-0696), Fe_3O_4 (19-0629)), OM/Ni:Co:Fe(Cl) (1 : 1 : 1) ($FeNi_3$ (65-3244) or a β-Co-based solid solution (15-0806), residual Ni(Co)Fe_2O_4 solid solution), and OM/Ni:Co:Fe(N) (1 : 1 : 1) (CoFe (44-1433), $FeNi_3$ (38-0419), (Fe,Ni) (47-1417)). (Fe(Cl): the solution was prepared using ferric chloride; Fe(N): the solution was prepared using ferric nitrate).

Figures 2 and 3 show TEM micrographs of the OM/Co (Fig. 2a), OM/Ni (Fig. 2b), and OM/Fe_3O_4 (Figs. 2c, 2d) nanocomposites and SEM micrographs of the unfilled opal (Fig. 3a) and OM/Ni nanocomposite (Fig. 3b). The electron micrographs of the OM nanocomposites illustrate the morphology of the iron group metal nanoparticles both on the surface of the silica spheres and in the opal pores. The cobalt metal nanoparticles are present not only as isometric crystals ranging in size from 10 to 70 nm but also as highly dispersed filamentary structures resembling pyrophoric cobalt. The reduction of the nickel compounds in opal pores leads to the formation of crystalline Ni nanoparticles (10 to 20 nm in size) with a face-centered cubic cell ($a = 0.3523$ nm, sp. gr. *Fm*3*m*).

The magnetic properties of the three-dimensional OM composites containing Ni, Co, and Fe_3O_4 nanoparticles were studied previously [40, 41]. Microstructural analysis of the opal samples demonstrates that all of the magnetic particles reside in opal pores and on the surface of the monodisperse spherical silica particles. The distance between the magnetic particles is determined by the amount of the magnetic phase embedded in the composite, the structural perfection of the opal, and the diameter of the SiO_2 particles. All of the composites studied here exhibit ferromagnetic behavior with rather high coercivity. This means that, at room temperature, the particles are in a blocked state, as would be expected for particles tens to hundreds nanometers in size. To evaluate the magnetic

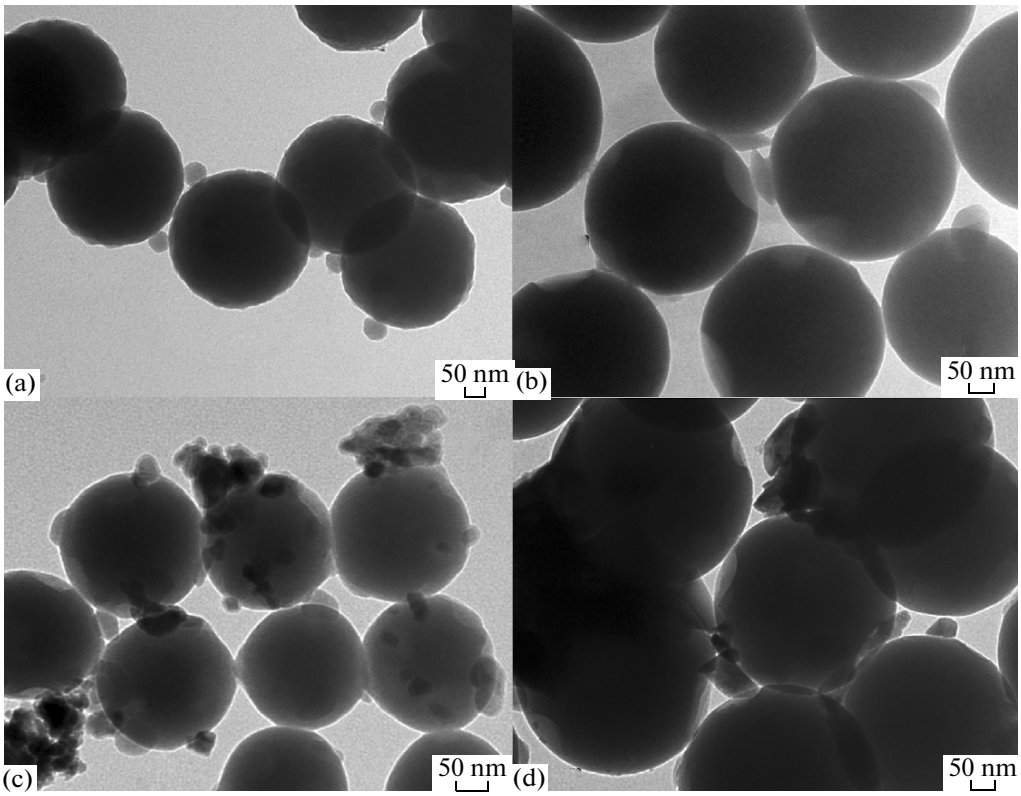

Fig. 2. TEM micrographs of the (a) OM/Co, (b) OM/Ni, and (c, d) OM/Fe_3O_4 nanocomposites.

moment of the nanoparticles, the experimental magnetization versus external field, $M(H)$, data for our samples at magnetic fields above 320 kA/m were fitted by the high-field limit of the Langevin function of the form

$$M(H) = M_s(1 - kT/m\mu_0 H), \quad (1)$$

where M_s is the saturation magnetization, T is the absolute temperature, m is the magnetic moment of the particles, k is Boltzmann's constant, and μ_0 is the permeability of vacuum. Figure 4 shows the $M(H)$ curves of the composites, normalized to the saturation magnetization. In the range 10–300 K, the temperature dependences of magnetic susceptibility for the OM:Fe, OM:Fe_3O_4, OM:Co(hex), OM:Co(cub), OM:Ni + NiO(cub), and OM:Ni(cub) composites do not have any anomalies.

The saturation magnetization (M_s), coercive force (H_c), and effective magnetic moment of the particles (m) are 6–10 A m^2/kg, 44 960 A/m, and 5075 μ_B in the OM/Co nanocomposite and 3–4 A m^2/kg, 19 890 A/m, and 19 400 μ_B in the OM/Ni nanocomposite. The low specific magnetic moments are due to the low concentrations of the metallic phase (several percent) in our samples, prepared by reducing thermal decomposition products with supercritical alcohols after a single cycle of filling the opal pores with 10 to 20% salt solutions. The highest coercive force was offered by the Co-containing samples, which correlates with the high magnetic anisotropy energy of metallic cobalt. The high coercive force and low effective magnetic moment of the particles may be caused by the considerable oxidation of the cobalt particles in the sample studied.

The composite samples containing Ni metal particles showed the highest saturation rate. The effective magnetic moment of the particles as determined using relation (1) has the maximum value. This is in perfect agreement with micrographs, which demonstrate that the size of the nickel particles markedly exceeds that of the nanoparticles in the other samples.

Figure 5a shows the reflection spectra of the as-prepared opal, with a sphere diameter near 270 nm, filled with air (spectrum *1*) or ethanol (spectrum *2*). Figures 5b–5f present the reflection spectra of the opal samples filled with nickel and air (Fig. 5b); cobalt and air (Fig. 5c); iron and air (Fig. 5d); nickel, cobalt, and air (Fig. 5e); and nickel, cobalt, iron, and air (Fig. 5f).

The presence of observed bands in the visible range in the broadband reflection spectra of the (111) surface of the OM composites is attributable to the formation of so-called band gaps in the photonic crystals. As a result, the spectrum of the dispersion curves of electromagnetic waves propagating in the [111] direction has a "gap," at which an electromagnetic wave cannot penetrate the material and reflects from its surface. For this crystallographic direction, we can use a one-dimensional model for a bilayer photonic crystal

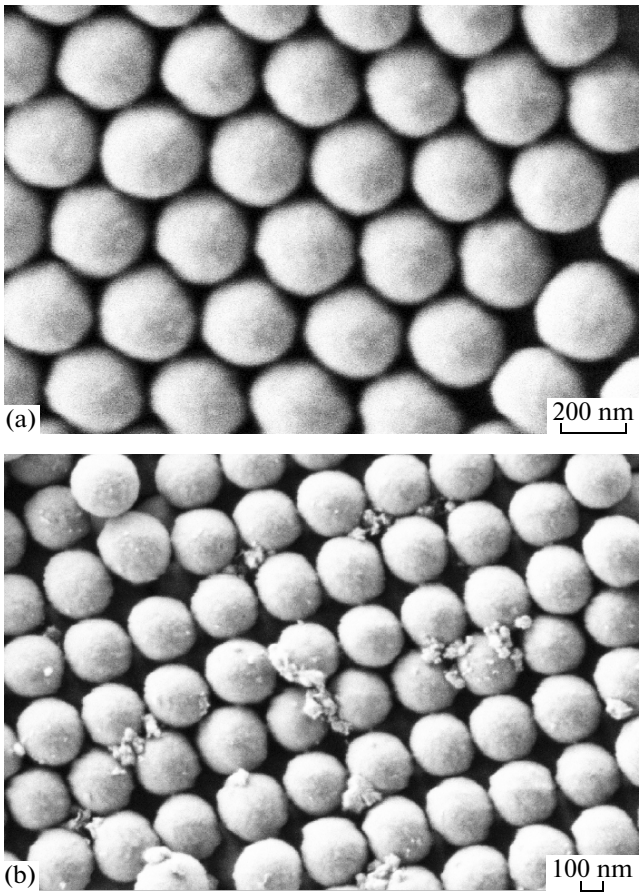

Fig. 3. SEM micrographs of thin cleaved specimens of the nanocomposites: (a) unfilled opal, (b) OM/Ni.

[42], in which the dispersion law $\omega(k)$ in implicit form is given by the relation

$$\cos(k_1a_1)\cos(k_2a_2) - \frac{1}{2}\left(\frac{n_1}{n_2} + \frac{n_2}{n_1}\right) \times \sin(k_1a_1)\sin(k_2a_2) = \cos(ka). \quad (2)$$

Here, $k_1 = (\omega/c)n_1$, $k_2 = (\omega/c)n_2$, n_1 and n_2 are the corresponding refractive indices of the two kinds of layers, a_1 and a_2 are the thicknesses of the layers, and $a = a_1 + a_2$ is the lattice parameter of the one-dimensional photonic crystal. The broadband reflection spectrum of the surface of the photonic crystals under consideration can be calculated using the formula

$$R(\omega) = \left|\frac{k(\omega) - \frac{\omega}{c}}{k(\omega) + \frac{\omega}{c}}\right|^2. \quad (3)$$

Here, the function $k(\omega)$ can be calculated using (2) and the refractive indices n_1 and n_2 of the layers. In accordance with the volume fraction of pores in the three-dimensional photonic crystal under consideration, we take $a_1 = 0.74a$ and $a_2 = 0.26a$. The refractive index of the SiO_2 spheres is taken to be $n_1 = 1.36$ [43]. It follows from relations (2) and (3) that the spectral width of the band gap can be evaluated using the formula

$$\frac{\Delta\lambda}{\lambda_0} \simeq \frac{\pi}{2}\frac{\Delta n}{n_{\text{eff}}}. \quad (4)$$

Here, $\Delta n = |n_1 - n_2|$; $\Delta\lambda$ is the spectral width of the band gap; λ_0 is the center wavelength of the band gap, $\lambda_0 = 2an_{\text{eff}}$; and $n_{\text{eff}}^2 = n_1^2 0.74 + n_2^2 0.26$. The incorpo-

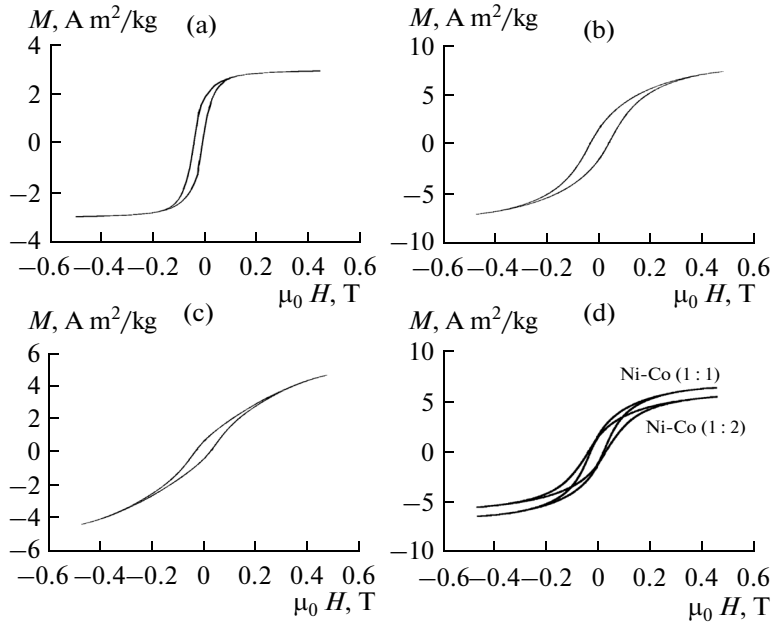

Fig. 4. Room-temperature $M(H)$ curves of the magnetic photonic crystals: (a) Ni/OM, (b) mixture of cubic and hexagonal Co/OM, (c) cubic Co/OM, (d) NiCo/OM.

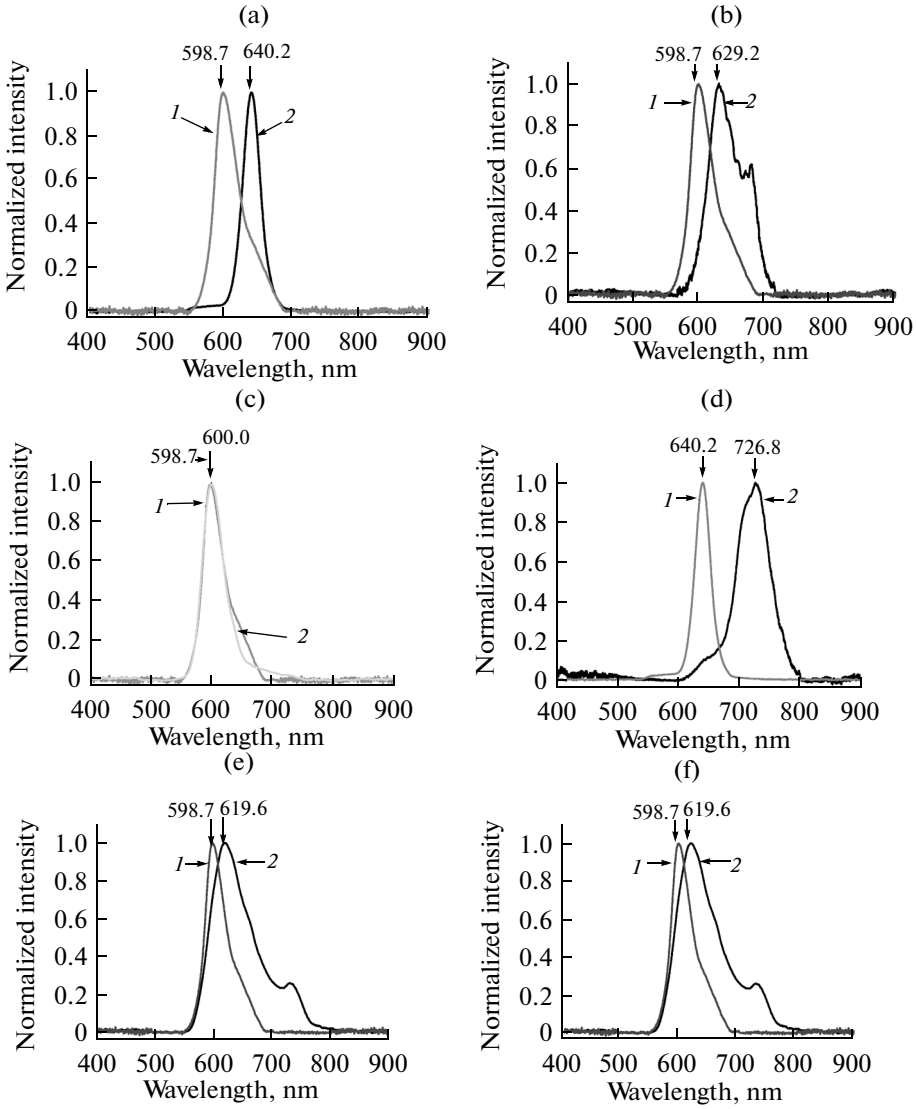

Fig. 5. Normalized broadband reflection spectra of the (111) surface of synthetic opal samples with a sphere diameter near 270 nm (measurements with a halogen lamp): (*1*) as-prepared, air-filled sample; (*2*) samples filled with (a) ethanol, (b) nickel + air, (c) cobalt + air, (d) iron + air, (e) nickel + cobalt + air, and (f) nickel + cobalt + iron + air.

ration of dielectric and metallic particles into opal pores changes n_2 and, accordingly, the effective refractive index n_{eff}, leading to a spectral shift of the experimentally observed maximum in the spectral intensity of the reflected light (Fig. 5). Note that the spectral width of the observed bands depends on the refractive index contrast $\Delta n = |n_1 - n_2|$. As seen from the spectra presented in Fig. 5, the index contrast is highest in the iron-filled opal and lowest in the cobalt-filled opal. The reflection spectra of some of our samples have a complex shape (Figs. 5b, 5e, 5f), suggesting nonuniform filling of the opal pores. According to experimental data, the observed spectra of a particular sample varied significantly from point to point, which also suggests that the opal-based nanocomposites were inhomogeneous.

Note also that, in contrast to the short-wavelength shift of the reflection peaks of opal crystals filled with gold and silver [7], in our OM/M (M = Fe, Co, Ni) samples, as seen in Fig. 5, the band gap exhibits an "anomalous" shift to longer wavelengths (like in opal filled with dielectrics, which have dielectric permittivity with a positive real part). It is reasonable to assume that the observed anomalous shift of the band gap in the opal crystals filled with 3*d* transition metal particles is due to the resonance dielectric permittivity dispersion in the visible range in the ferromagnets containing *d* electrons.

CONCLUSIONS

The present results demonstrate that, by reducing salts and oxides with supercritical isopropanol at temperatures no higher than 270°C and pressures under 10 MPa, one-, two-, and three-component iron group metal (Fe, Co, Ni) nanoparticles ranging in size from 10 to 60 nm can be produced in opal pores.

The composition of the starting salts (nitrates and chlorides) is shown to influence the phase composition of the OM/M composites. In the binary system of Ni and Co nitrates (1 : 1), exposure of opal to supercritical isopropanol leads to the formation of particles of a cubic solid solution with the composition NiCo. In the Ni–Fe and Co–Fe systems, the infiltration of opal with ferric chloride leads to the formation of nanoparticles of solid solutions based on nickel metal, α-cobalt, or β-cobalt and oxides or an MFe_2O_4 spinel phase. After the supercritical isopropanol reduction of the composites filled with Fe, Ni–Fe, and Co–Fe nitrates, we identified for the first time, in addition to spinel phases, iron metal and intermetallic nanoparticles with a regular metal atom distribution: Ni_3Fe, NiFe, and CoFe. The supercritical isopropanol reduction of the composites produced by heat-treating a ternary mixture of nickel nitrate, cobalt nitrate, and ferric chloride leads to the formation of nanoparticles of a NiCoFe solid solution with an fcc structure and an oxide phase with the spinel structure in the opal pores. In the case of the OM composite filled with a ternary system of Ni–Co–Fe nitrates (1 : 1 : 1), we found almost complete reduction of the spinel phases to the intermetallic compounds Ni_3Fe, NiFe, and CoFe.

Analysis of the reflection spectra of the (111) surface of the magnetic nanocomposites produced in this study demonstrates that the incorporation of iron group metal nanoparticles into opal pores changes the shape and spectral position of the reflection band of the as-prepared (air-filled) opal. Analysis of the reflection spectra of different areas on the (111) surface of the photonic crystals studied here indicated nonuniform filling of the opal pores. The procedure for incorporating metallic nanoparticles into opal pores can be improved further by optimizing filling conditions and analyzing the homogeneity of the material using the proposed fiber-optic technique for local evaluation of the spectral position of band gaps. The photonic crystals produced in this study, containing magnetic metallic nanoparticles, can be used for controlling the reflection spectrum of magnetic photonic crystals by an external magnetic field by virtue of the magneto-optical effect.

ACKNOWLEDGMENTS

This work was supported by the Russian Foundation for Basic Research, grant nos. 12-02-00563, 13-02-00662, and 14-02-90406.

REFERENCES

1. Gaponenko, S.V., Kapitonov, A.M., Bogomolov, V.N., Prokofiev, A.V., Eychmuller, A., and Rogach, A.L., Electrons and photons in mesoscopic structures: quantum dots in a photonic crystal, *JETP Lett.*, 1998, vol. 68, no. 2, pp. 131–135.
2. Golubev, V.G., Kurdyukov, D.A., and Pevtsov, A.B., Three-dimensional photonic crystals based on opal–semiconductor nanocomposites, *Fundamental'nye problemy optiki. Trudy konferentsii* (Proc. Conf. Fundamental Issues in Optics, St. Petersburg, 2002), St. Petersburg: SPbGITMO, 2002, p. 90.
3. Romanov S.G. Light propagation in nonuniform colloidal photonic crystals, *Extended Abstract of Doctoral (Phys.–Math.) Dissertation*, St. Petersburg: Ioffe Physicotechnical Inst., Russ. Acad. Sci., 2013.
4. Baryshev, A.V., Kaplyanskii, A.A., Kosobukin, V.A., Limonov, M.F., and Skvortsov, A.P., Spectroscopy of the photonic stop band in synthetic opals, *Phys. Solid State*, 2004, vol. 46, no. 7, pp. 1331–1339.
5. Gorelik, V.S., Optics of globular photonic crystals, *Laser Phys.*, 2008, vol. 18, no. 12, pp. 1479–1500.
6. Avakyants, L.P., Gorelik, V.S., Zlobina, L.I., Mel'nik, N.N., Sverbil', P.P., Fadyushin, A.B., and Chervyakov, A.V., Raman scattering study of $NaNO_2$-infiltrated opal photonic crystals, *Inorg. Mater.*, 2006, vol. 41, no. 6, pp. 635–640.
7. Gorelik, V.S., Optical and dielectric properties of nanostructured photonic crystals loaded by ferroelectrics and metals, *Phys. Solid State*, 2009, vol. 51, no. 7, pp. 1321–1327.
8. Gubin, S.P., Koksharov, Yu.A., Khomutov, G.B., and Yurkov, G.Yu., Magnetic nanoparticles: preparation, structure, and properties, *Usp. Khim.*, 2005, vol. 74, no. 6, pp. 539–574.
9. Han, Y.C., Cha, H.G., Kim, C.W., Kim, Y.H., and Kang, Y.S., Synthesis of highly magnetized iron nanoparticles by a solventless thermal decomposition method, *J. Phys. Chem. C*, 2007, vol. 111, no. 17, pp. 6275–6280.
10. Bao, N., Shen, L., Wang, Y., Padhan, P., and Gupta, A., A facile thermolysis route to monodisperse ferrite nanocrystals, *J. Am. Chem. Soc.*, 2007, vol. 129, no. 41, pp. 12 374–12 375.
11. Sapoletova, N.A., Napol'skii, K.S., Gorozhankin, D.F., Eliseev, A.A., and Mishina, E.D., Electrochemical engineering of photonic crystal materials, *Opalopodobnye struktury: Sbornik trudov vserossiiskoi konferentsii* (Opal-Like Structures: Proc. All-Russia Conf.), St. Petersburg, 2010, pp. 111–113.
12. Zakharov, Yu.A., Popova, A.N., Pugachev, V.M., and Dodonov, V.G., Some properties of iron–cobalt and iron–nickel nanopowders, *Polzunov. Vestn.*, 2008, no. 3, pp. 79–83.
13. Sviridov, V.V., *Khimicheskoe osazhdenie metallov iz vodnykh rastvorov* (Chemical Deposition of Metals from Aqueous Solutions), Minsk: Universitetskoe Izd., 1987.
14. Pileni, M.P., Reverse micelles: a microreactor, *J. Phys. Chem.*, 1993, vol. 97, no. 27, pp. 9661–9668.
15. Ban, I., Drofenik, M., and Makovec, D., The synthesis of iron–nickel alloy nanoparticles using a reverse micelle technique, *J. Magn. Magn. Mater.*, 2006, vol. 307, no. 2, pp. 250–256.

16. Liu, X., Chun, C.M., Aksay, I.A., and Shih, W.H., Synthesis of mesostructured nickel oxide with silica, *Ind. Eng. Chem. Res.*, 2000, vol. 39, no. 3, pp. 684–692.
17. Grigor'ev, S.V., Chumakov, A.P., Syromyatnikov, A.V., Grigor'eva, N.A., Okorokov, A.I., Napol'skii, K.S., Roslyakov, I.V., Eliseev, A.A., Lukashin, A.V., and Ekkerlebe Khyu, Magnetic properties of a two-dimensional spatially ordered array of nickel nanowires, *Phys. Solid State*, 2010, vol. 52, no. 5, pp. 1080–1086.
18. Gao, Y., Zingaro, R.A., and Gao, M.Z., A silica immobilized cobalt complex: absorption of dioxigen and the redox ability in aqueous solution, *Polyhedron*, 2004, vol. 23, no. 1, pp. 59–62.
19. Napol'skii, K.S., Kolesnik, I.V., Eliseev, A.A., Lukashin, A.V., Vertegel, A.A., and Tret'yakov, Yu.D., Synthesis of filamentary iron nanoparticles in a mesoporous silica matrix, *Dokl. Chem.*, 2002, vol. 386, nos. 1–3, pp. 242–245.
20. Zakharov, Yu.A., Popova, A.N., and Pugachev, V.M., Phase composition of iron–cobalt nanopowders, *Polzunov. Vestn.*, 2009, no. 3, pp. 60–63.
21. Chaubey, G.S., Barcena, C., Poudyal, N., Rong, C., Gao, J., Sun, S., and Liu, J.P., Synthesis and stabilization of FeCo nanoparticles, *J. Am. Chem. Soc.*, 2007, vol. 129, no. 41, pp. 7214–7215.
22. Liao, Q., Tannenbaum, R., and Wang, Z.L., Synthesis of $FeNi_3$ alloyed nanoparticles by hydrothermal reduction, *J. Phys. Chem. B*, 2006, vol. 110, no. 29, pp. 14 262–14 265.
23. Peng, S., Wang, C., Xie, J., and Sun, S., Synthesis and stabilization of monodisperse Fe nanoparticles, *J. Am. Chem. Soc.*, 2006, vol. 128, no. 33, pp. 10 676–10 677.
24. Cozzoli, P.D., Snoeck, E., Garcia, M.A., Giannini, C., Guagliardi, A., Cervellino, A., Gozzo, F., Hernando, A., Achterhold, K., Ciobanu, N., Parak, F.G., Cingolani, R., and Manna, L., Colloidal synthesis and characterization of tetrapod-shaped magnetic nanocrystals, *Nanoletters*, 2006, vol. 6, no. 9, pp. 1966–1972.
25. Desvaux, C., Amiens, C., Fejes, P., Renaud, P., Respaud, M., Lecante, P., Snoeck, E., and Chaudret, B., Multimillimetre-large superlattices of air-stable iron–cobalt nanoparticles, *Nat. Mater.*, 2005, vol. 4, no. 10, pp. 750–753.
26. Yamauchi, T., Tsukahara, Y., Yamada, K., Sakata, T., and Wada, Y., Nucleation and growth of magnetic Ni–Co (core–shell) nanoparticles in a one-pot reaction under microwave irradiation, *Chem. Mater.*, 2011, vol. 23, no. 1, pp. 74–84.
27. Bulygina, E.V., Marchuk, V.V., Panfilov, Yu.V., Oya, D.R., and Shakhnov, V.Ya., *Nanorazmernye struktury: klassifikatsiya, formirovanie i issledovanie* (Nanostructures: Classification, Formation, and Characterization), Moscow: SAINS-PRESS, 2006.
28. Bozhko, S.I., Naumenko, I.G., Samorov, E.N., Masalov, V.M., Emel'chenko, G.A., Ionov, A.M., and Fokin, D.A., Formation of two-dimensional ordered magnetic nanolattices in opal structures, *JETP Lett.*, 2004, vol. 80, no. 7, pp. 500–502.
29. Gorelik, V.C., Ionin, A.A., Kudryashov, S.I., Makarov, S.V., Seleznev, L.V., Sinitsyn, D.V., Chanieva, F.A., and Sharipov, A.F., Opal-based nanocomposites produced by laser ablation using femtosecond laser pulses, *Kratk. Soobshch. Fiz.*, 2011, no. 11, pp. 20–29.
30. Tret'yakov, Yu.D., Lukashin, A.V., and Eliseev, A.A., Synthesis of functional nanocomposites based on solid-state nanoreactors, *Usp. Khim.*, 2004, vol. 73, no. 9, pp. 974–998.
31. Yu, X., Lee, Yu.-J., Furstenberg, R., White, J.O., and Braun, P.V., Filling fraction dependent properties of inverse opal metallic photonic crystals, *Adv. Mater.*, 2007, vol. 19, no. 13, pp. 1689–1692.
32. Kargin, Yu.F., Ivicheva, S.N., Buslaeva, E.Yu., Kuvshinova, T.B., Volodin, V.D., and Yurkov, G.Yu., Preparation of bismuth nanoparticles in opal matrices through reduction of bismuth compounds with supercritical isopropanol, *Inorg. Mater.*, 2006, vol. 42, no. 5, pp. 487–490.
33. Kargin, Yu.F., Ivicheva, S.N., Buslaeva, E.Yu., Yurkov, G.Yu., and Volodin, V.D., Reduction of various metal salts in opal matrices with supercritical isopropanol, *Inorg. Mater.*, 2006, vol. 42, no. 9, pp. 966–970.
34. Ivicheva, S.N. and Kargin, Yu.F., Ordered opal-matrix nanocomposites containing iron group metal nanoparticles, *Institut metallurgii i materialovedeniya im. A.A.Baikova RAN – 75 let. Sbornik nauchnyk trudov* (Baikov Institute of Metallurgy and Materials Science, Russian Academy of Sciences—75 Years: A Collection of Scientific Papers), Solntsev, K.A., Ed., Moscow: Nauka, 2013, pp. 743–761.
35. Ivicheva, S.N., Kargin, Yu.F., Ashmarin, A.A., Shvorneva, L.I., and Ivanov, V.K., Nanocomposites based on opal matrices and iron subgroup metal nanoparticles, *Russ. J. Inorg. Chem.*, 2012, vol. 57, no. 11, pp. 1419–1427.
36. Gorelik, V.S., Zlobina, L.I., Troitskii, O.A., Chanieva, R.I., Emission spectra of silver-infiltrated opal photonic crystals under excitation through optical fibers, *Inorg. Mater.*, 2009, vol. 45, no. 7, pp. 785–790.
37. Voinov, Yu.P., Gorelik, V.S., Zlobina, L.I., and Filatov, V.V., Reflectivity spectra of gold- and silver-infiltrated opals, *Inorg. Mater.*, 2009, vol. 45, no. 10, pp. 1133–1138.
38. Ivicheva, S.N., Kargin, Yu.F., Shvorneva, L.I., Kutsev, S.V., and Yurkov, G.Yu., Ni, Co, Cu, Ni–Co, and Ni–Cu nanoparticles in opal matrices and mesoporous silica gels, *Inorg. Mater.*, 2012, vol. 48, no. 3, pp. 289–297.
39. *PCPDFWIN v. 2.4*, JCPDS–International Centre for Diffraction Data, 2003.
40. Ivicheva, S.N., Kargin, Yu.F., Ovchenkov, E.A., Koksharov, Yu.A., and Yurkov, G.Yu., Properties of three-dimensional composites based on opal matrices and magnetic nanoparticles, *Phys. Solid State*, 2011, vol. 53, no. 6, pp. 1114–1120.
41. Ivicheva, S.N., Kargin, Yu.F., Ovchenkov, E.A., and Koksharov, Y.A., 3D composites based on opal matrix and heterometallic nanoparticles, *12th China–Russia Symp. on Advanced Materials and Technologies*, part I: *Advanced Metals, Ceramics and Composites*, Kunming: Yunnan, 2013, pp. 26–30.
42. Yariv, A. and Yeh, P., *Optical Waves in Crystals: Propagation and Control of Laser Radiation*, Hoboken: Wiley, 2003.
43. Malitson, I.H., Interspecimen comparison of the refractive index of fused silica, *J. Opt. Soc. Am.*, 1965, vol. 55, no. 10, pp. 1205–1208.

Translated by O. Tsarev